

Article

## New Layered Oxide-Fluoride Perovskites: $\text{KNaNbOF}_5$ and $\text{KNaMO}_2\text{F}_4$ ( $M = \text{Mo}^{6+}, \text{W}^{6+}$ )

Rachelle Ann F. Pinlac, Charlotte L. Stern and Kenneth R. Poeppelmeier \*

Department of Chemistry, Northwestern University, 2145 Sheridan Road, Evanston, IL 60208, USA;  
E-Mails: r-pinlac@u.northwestern.edu (R.A.F.P.); c-stern@northwestern.edu (C.L.S.)

\* Author to whom correspondence should be addressed; E-Mail: krp@northwestern.edu;  
Tel.: +1-847-491-3505; Fax: +1-847-491-7713.

Received: 24 February 2011; in revised form: 9 March 2011 / Accepted: 16 March 2011 /  
Published: 18 March 2011

---

**Abstract:**  $\text{KNaNbOF}_5$  and  $\text{KNaMO}_2\text{F}_4$  ( $M = \text{Mo}^{6+}, \text{W}^{6+}$ ), three new layered oxide-fluoride perovskites with the general formula  $\text{ABB}'\text{X}_6$ , form from the combination of a second-order Jahn-Teller  $d^0$  transition metal and an alkali metal ( $\text{Na}^+$ ) on the B-site. Alternating layers of cation vacancies and  $\text{K}^+$  cations on the A-site complete the structure. The  $\text{K}^+$  cations are found in the A-site layer where the fluoride ions are located. The A-site is vacant in the adjacent A-site layer where the axial oxides are located. This unusual layered arrangement of unoccupied A-sites and under bonded oxygen has not been observed previously although many perovskite-related structures are known.

**Keywords:** perovskites; oxide-fluorides; hydrothermal synthesis

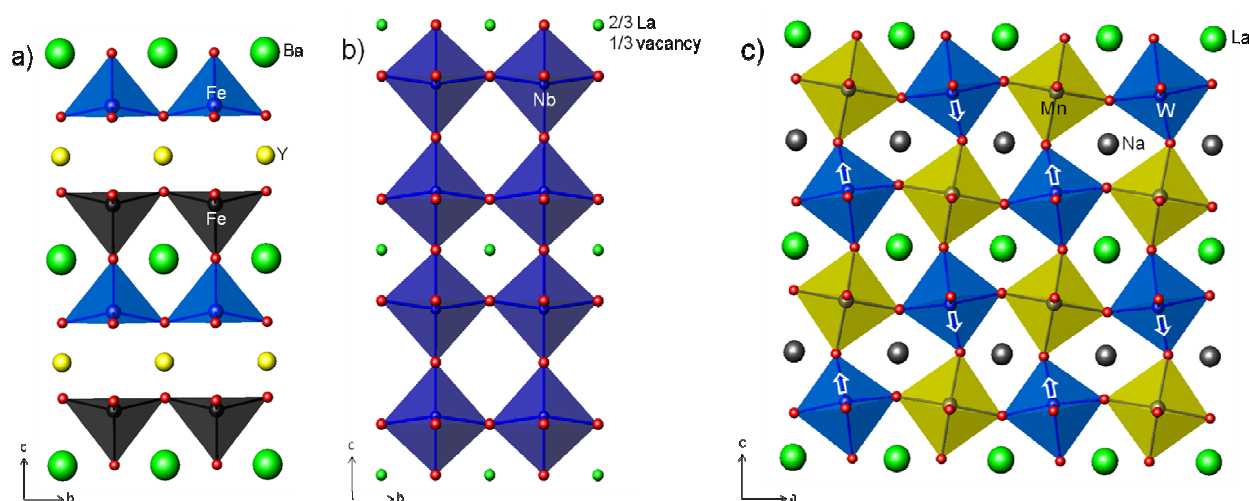
---

### 1. Introduction

Perovskites with the general formula  $\text{ABX}_3$  are some of the most studied structures owing to their many interesting properties including magnetism, ionic conductivity, and ferroelectricity [1-3]. Their structure and properties can be altered by substitution at either the A- or B-sites or creating either cation or anion vacancies. For example, ferromagnetism has been achieved with the complex perovskite  $\text{AA}'_3\text{B}_4\text{O}_{12}$ , such as  $\text{CaCu}_3\text{Ge}_4\text{O}_{12}$  [1], and ionic conductivity has been observed for the A-site deficient perovskites  $\text{Li}_{3x}\text{La}_{(2/3-x)}\square_{1/3-2x}\text{TiO}_3$  ( $0 < x < 0.16$ ) [2].

A-site cation ordering is typically seen in anion deficient perovskites, such as the antiferromagnetic  $\text{YBaFe}_2\text{O}_5$  where the A-site cations ( $\text{Y}^{3+}$  and  $\text{Ba}^{2+}$ ) are ordered owing to the oxygen vacancies (Figure 1a) [4]. Ordered layers of occupied and unoccupied A-sites occur in non-stoichiometric perovskites  $\text{A}_{1-x}\text{BO}_3$  [5-8]. For example,  $\text{La}_{1/3}\text{NbO}_3$  contains a  $\text{ReO}_3$  framework of  $\text{NbO}_6$  octahedra with unoccupied A-site layers and A-site layers occupied with  $2/3$  La alternating along  $c$  (Figure 1b) [6,7]. Examples of A-site cation ordering in stoichiometric  $\text{AA}'\text{B}_2\text{X}_6$  and  $\text{AA}'\text{BB}'\text{X}_6$  perovskites with neither anion vacancies nor A-site vacancies are rare [9]. Woodward *et al.* showed that in  $\text{NaLnMnWO}_6$  ( $\text{Ln} = \text{Ce}, \text{Pr}, \text{Sm}, \text{Gd}, \text{Dy}$  and  $\text{Ho}$ ) and  $\text{NaLnMgWO}_6$  ( $\text{Ln} = \text{Ce}, \text{Pr}, \text{Sm}, \text{Gd}, \text{Tb}, \text{Dy}$  and  $\text{Ho}$ ) the A-site cations Na and Ln prefer to order in a layered arrangement [10,11]. The layered A-site ordering is stabilized by the second order Jahn Teller displacement of the  $d^0$  transition metal W at the B-site towards the oxide that is under bonded to alleviate the lattice strain arising from the A-site cations size mismatch (Figure 1c).

**Figure 1.** Structures of (a) anion deficient  $\text{YBaFe}_2\text{O}_5$  [4], (b) non-stoichiometric  $\text{La}_{1/3}\text{NbO}_3$  [6,7] and (c) stoichiometric  $\text{NaLaMnWO}_6$  [10,11].



In comparison, B-site cation ordering in  $\text{A}_2\text{BB}'\text{X}_6$  double perovskites has been well documented [12-14]. The majority of the B and B' cations crystallize in an ordered rock-salt structure. In general, a disordered arrangement is observed when the oxidation states of B and B' differ by less than two, whereas a difference greater than two nearly always produces an ordered arrangement [12]. When the difference in oxidation state is exactly two, disordered, partially ordered or fully ordered arrangements can result, depending on the differences in size and/or bonding preference of the B and B' cations [12,15,16].

Oxyfluoride perovskites that contain ordered oxide and fluoride ions with the general formula  $[\text{MO}_x\text{F}_{6-x}]^{n-}$  ( $x = 1, n = 2$ , and  $M = \text{V}^{5+}, \text{Nb}^{5+}, \text{Ta}^{5+}$ ;  $x = 2, n = 2$ , and  $M = \text{Mo}^{6+}, \text{W}^{6+}$ ;  $x = 2, n = 3$ , and  $M = \text{V}^{5+}, \text{Nb}^{5+}, \text{Ta}^{5+}$ ;  $x = 3, n = 3$ , and  $M = \text{Mo}^{6+}$ ) are known but not common [17]. One well known example  $\text{Na}_3\text{MoO}_3\text{F}_3$ , which crystallizes in the cryolite structure and has ordered oxide and fluoride ligands, displays ferroelectric-ferroelastic properties [3]. In this paper, we report a new class of A-site deficient oxyfluoride perovskites  $\text{ABMO}_x\text{F}_{6-x}$  (where  $\text{A} = \text{K}^+$ ;  $\text{B} = \text{Na}^+$ ;  $x = 1, M = \text{Nb}^{5+}$ ;  $x = 2, M = \text{Mo}^{6+}, \text{W}^{6+}$ ) that crystallize with both A- and B-site ordered cations.  $\text{KNaNbOF}_5$  [18] and

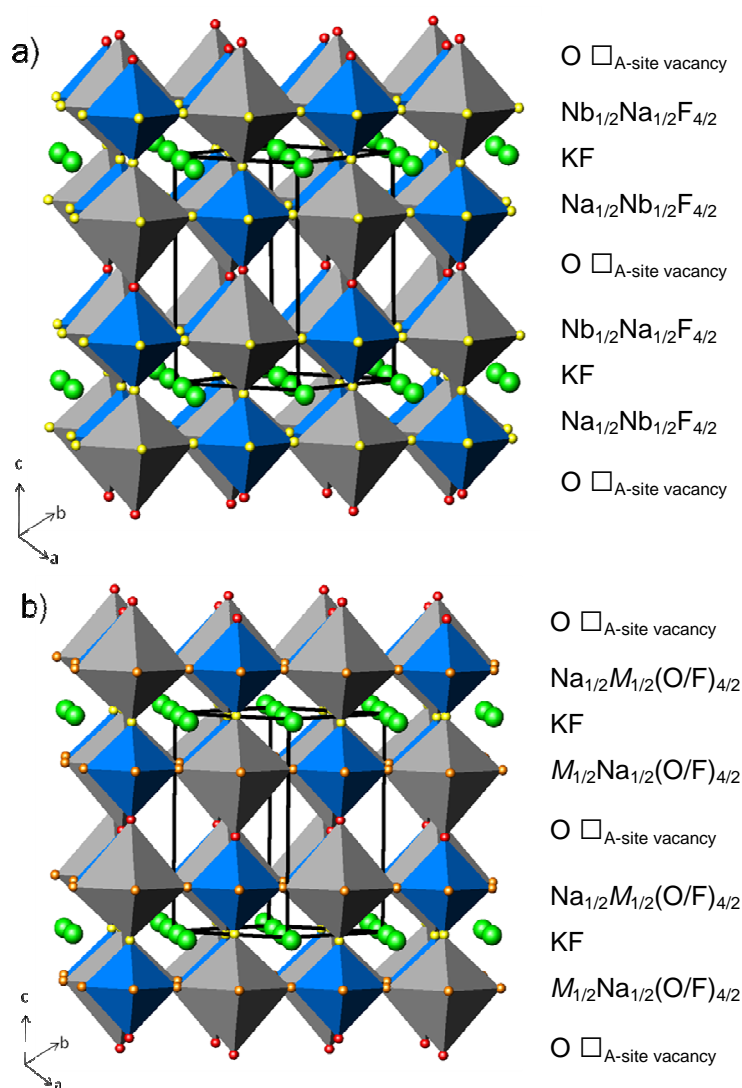
$\text{KNaMO}_2\text{F}_4$  ( $M = \text{Mo}^{6+}, \text{W}^{6+}$ ) have a rock-salt ordering of the B-site Na and Nb/ $M$  cations. The A-sites are arranged in a layered manner where one A-site layer contains all of the  $\text{K}^+$  cations and in the adjacent layer the A-sites are completely vacant.

## 2. Results and Discussion

### 2.1. Structure description

The polyhedral representations of  $\text{KNaNbOF}_5$  and  $\text{KNaMO}_2\text{F}_4$  ( $M = \text{Mo}^{6+}, \text{W}^{6+}$ ) are shown in Figure 2. These three-dimensional structures can be described as an ordered rock-salt double perovskite with the general formula  $\text{ABB}'\text{X}_6$  with ordered A-site layers where  $\text{K}^+$  occupies half the A-sites and  $\text{Na}^+$  and  $\text{Nb}^{5+}$  or  $M^{6+}$  occupy the B and B' sites, respectively. X represents one  $\text{O}^{2-}$  and five F in  $\text{KNaNbOF}_5$  and two  $\text{O}^{2-}$  and four F in  $\text{KNaMO}_2\text{F}_4$ . Note that throughout the following discussion  $M$  corresponds to either molybdenum or tungsten atoms.

**Figure 2.** View of the three dimensional rock salt double perovskite (a)  $\text{KNaNbOF}_5$  and (b)  $\text{KNaMO}_2\text{F}_4$  ( $M = \text{Mo}^{6+}, \text{W}^{6+}$ ). Blue octahedra represent the  $[\text{NbOF}_5]^{2-}$  or  $[\text{MO}_2\text{F}_4]^{2-}$  units, grey octahedra represent Na-centered units and green spheres represent  $\text{K}^+$  ions.



In  $\text{KNaNbOF}_5$ , the  $\text{Na}^+$  and  $\text{Nb}^{5+}$  ions occupy ordered corner-shared octahedra (no tilt,  $a^0a^0a^0$ ) as in the  $\text{ReO}_3$  structure type. The  $\text{Nb}^{5+}$  ions form short  $\text{Nb}=\text{O}$  bonds and one long  $\text{Nb}-\text{F}$  bond *trans* to the oxide (Table 1) resulting in a distorted octahedron, as seen in previously reported  $d^0$  transition metal anionic units [19,20]. Mid-IR confirms the presence of the  $\text{Nb}=\text{O}$  bond with a peak at  $\nu_s$   $975\text{ cm}^{-1}$  [21]. The  $\text{Nb}-\text{O}-\text{Na}$  and  $\text{Nb}-\text{F}_2-\text{Na}$  bond angles are  $180^\circ$  along the *c*-axis (Table 1), consistent with corner sharing octahedra with no tilt. The  $\text{Nb}-\text{F}_3-\text{Na}$  bond angle is  $162.50(4)^\circ$ .

In  $\text{KNaMO}_2\text{F}_4$ , the oxide ion and its *trans* fluoride are ordered. The second oxide ion is disordered among the other three fluorides in the equatorial positions. Although this partial ordering occurs between the oxide and fluoride ions, the A- and B-site cations are both ordered. The B-site cations,  $\text{Na}^+$  and  $M^{6+}$ , form corner-sharing octahedra (no tilt,  $a^0a^0a^0$ ). The  $M^{6+}$  ions form one short  $M=\text{O}$  and one long  $M-\text{F}$  bond *trans* to the oxide (Table 1) and, as a result, distort toward the corners of the octahedra as opposed to the edges [22,23]. Mid-IR confirms the presence of the  $M=\text{O}$  bond with peaks at  $\nu_s$   $969\text{ cm}^{-1}$  and  $\nu_{\text{as}}$   $916\text{ cm}^{-1}$  for Mo and  $\nu_s$   $991\text{ cm}^{-1}$  and  $\nu_{\text{as}}$   $923\text{ cm}^{-1}$  for W [21]. Again, the  $M-\text{O}-\text{Na}$  and  $M-\text{F}_2-\text{Na}$  bond angles are  $180^\circ$  along the *c*-axis consistent with corner-shared octahedra with no tilt. The  $M-\text{X}_3-\text{Na}$  bond angle is  $164.03(5)^\circ$  and  $162.11(8)^\circ$  for Mo and W, respectively.

The A-site  $\text{K}^+$  cations occupy half of the positions in an ordered array. Along the *c*-axis, the  $\text{K}^+$  cations are 12-coordinated to the  $\text{F}^-$  in the A-site layer. In the adjacent layer, where the axial oxides are located, the A-site is vacant. The unique  $\text{ABB}'\text{X}_6$  structure can be described as repeating AX layers of  $\text{KF}$ ,  $\text{BX}_2$  layers of  $\text{Na}_{1/2}\text{Nb}_{1/2}\text{F}_{4/2}$ , X layers of O,  $\text{BX}_2$  layers of  $\text{Na}_{1/2}\text{Nb}_{1/2}\text{F}_{4/2}$ , *etc* (Figure 2a) for  $\text{KNaNbOF}_5$ .  $\text{KNaMO}_2\text{F}_4$  can be described as repeating AX layers of  $\text{KF}$ ,  $\text{BX}_2$  layers of  $\text{Na}_{1/2}M_{1/2}(\text{O}/\text{F})_{4/2}$ , X layers of O,  $\text{BX}_2$  layers of  $\text{Na}_{1/2}M_{1/2}(\text{O}/\text{F})_{4/2}$ , *etc*. (Figure 2b).

**Table 1.** Selected bond lengths and bond angles for  $\text{KNaNbOF}_5$  and  $\text{KNaMO}_2\text{F}_4$  ( $M = \text{Mo}, \text{W}$ ).

Bond Distances (Å)					
Nb-O	1.7179(14)	Mo-O	1.6718(16)	W-O	1.698(3)
Nb-F2	2.1473(11)	Mo-F2	2.1110(12)	W-F2	2.100(2)
Nb-F3 x 4	1.9552(7)	Mo-X3 x 4	1.9074(7)	W-X3 x 4	1.9033(13)
Na-O	2.2961(16)	Na-O	2.3408(17)	Na-O	2.298(3)
Na-F2	2.3501(14)	Na-F2	2.3360(14)	Na-F2	2.394(3)
Na-F3 x 4	2.2754(7)	Na-X3 x 4	2.2766(7)	Na-X3 x 4	2.2938(13)
Bond Angles					
O-Nb-F2	$180.00^\circ$	O-Mo-F2	$180.00^\circ$	O-W-F2	$180.00^\circ$
O-Nb-F3	$99.364(18)^\circ$	O-Mo-X3	$99.07(2)^\circ$	O-W-X3	$99.03(4)^\circ$
F2-Nb-F3	$80.636(18)^\circ$	F2-Mo-X3	$80.93(2)^\circ$	F2-W-X3	$80.97(4)^\circ$
Nb-O-Na	$180.00^\circ$	Mo-O-Na	$180.00^\circ$	W-O-Na	$180.00^\circ$
Nb-F2-Na	$180.00^\circ$	Mo-F2-Na	$180.00^\circ$	W-F2-Na	$180.00^\circ$
Nb-F3-Na	$162.50(4)^\circ$	Mo-X3-Na	$164.03(5)^\circ$	W-X3-Na	$162.11(8)^\circ$

## 2.2. Bond valence and anionic connectivity

Electronic potentials and chemical hardness cooperatively influence the long-range order of the  $[\text{NbOF}_5]^{2-}$  anionic unit [20,23]. Oxide and fluoride order can be understood in the context of Pauling's second crystal rule (PSCR) which states that anions with the largest negative potentials will occupy

sites having the largest positive potentials [24]. The assessment of the positive potential in the crystal frameworks, carried out by calculating the PSCR (bond strength) sum [25] and bond valence sum [24,26] around each anionic position, should match as closely as possible to the assessment of the negative potentials of each oxide and fluoride ion (Tables 2 and 3). The central Nb<sup>5+</sup> ion has been excluded from the PCSR calculations because we are only interested in the oxide and fluoride interactions with the extended bond network.

In a purely inorganic bond network, the oxide and fluoride ligands in the [NbOF<sub>5</sub>]<sup>2-</sup> anionic unit with the largest residual negative charge will make the most and strongest contacts to the coordination environment [20]. In KNaNbOF<sub>5</sub>, the F2 fluorides, which occupy positions in contact with one six-coordinate Na<sup>+</sup> and four twelve-coordinate K<sup>+</sup> (1/6 + 4 × 1/12 = 0.5 PSCR sum and bond valence sums of 0.46 vu), retain the most negative potentials (0.58 vu) (Table 3). The four remaining fluorides, F3, have less negative potentials (0.29 vu). They are each three-coordinate (one Na<sup>+</sup> and two K<sup>+</sup>) with lower bond valence sums of 0.40 vu and PSCR sums of 0.33.

**Table 2.** Bond lengths, experimental bond valences and bond valence sums for KNaNbOF<sub>5</sub>.

KNaNbOF <sub>5</sub>		K	Na	Nb	V <sub>i</sub> = Σ <sub>i</sub> S <sub>ij</sub>
R <sub>ij</sub> (Å)	O1		2.2961(16)	1.7179(14)	<b>1.95</b>
S <sub>ij</sub> (vu)			<b>0.26</b>	<b>1.69</b>	
R <sub>ij</sub> (Å)	F2	2.9586(9)	2.3501(14)	2.1473(11)	<b>0.88</b>
S <sub>ij</sub> (vu)		<b>0.07</b>	<b>0.16</b>	<b>0.42</b>	
R <sub>ij</sub> (Å)	F3	2.8492(4)	2.2754(7)	1.9552(7)	<b>1.11</b>
S <sub>ij</sub> (vu)		<b>0.10</b>	<b>0.20</b>	<b>0.71</b>	
V <sub>j</sub> = Σ <sub>j</sub> S <sub>ij</sub>		<b>1.08</b>	<b>1.22</b>	<b>4.95</b>	

R<sub>ij</sub> = bond length of the bond "ij"; S<sub>ij</sub> = exp[(R<sub>0</sub> - R<sub>ij</sub>)/B] experimental bond valence of bond "ij", where R<sub>0</sub> = constant dependent on *i* and *j* bonded elements, and B = 0.37; R<sub>0</sub>(Nb–O) = 1.911, R<sub>0</sub>(Nb–F) = 1.87; R<sub>0</sub>(Na–O) = 1.803, R<sub>0</sub>(Na–F) = 1.677; s<sub>ij</sub> = theoretical bond valence of bond "ij", calculated by solving the network equations based on the methods described by Brown [27,28]; V<sub>i</sub>, V<sub>j</sub> = experimental valences of anions "i" and cations "j"; z<sub>i</sub>, z<sub>j</sub> = charge or formal valence of anions "i" and cations "j".

**Table 3.** Estimations of the negative potentials of the ions of the (NbOF<sub>5</sub>)<sup>2-</sup> anions and the surrounding positive potentials in KNaNbOF<sub>5</sub>, through bond strength and bond valence calculations.

KNaNbOF <sub>5</sub>			
Bond	Anionic BV (vu) <sup>a</sup>	Cationic PSCR sum (vu) <sup>b</sup>	Cationic BV sum (vu) <sup>c</sup>
Nb–O1	0.31	0.17	0.26
Nb–F2	0.58	0.50	0.46
Nb–F3	0.29	0.33	0.40

<sup>a</sup> Anionic BV (Bond Valence) = z<sub>i</sub> - S<sub>Nb–O/F</sub>, where z<sub>i</sub> is the electric charge of each ligand and S<sub>Nb–O/F</sub> is taken from the Table 2 for each Nb–O/F bond; <sup>b</sup> Cationic PSCR sum = Σ<sub>j</sub> S'\_{j,cat} = Σ<sub>j</sub>  $\frac{z_{j,cat}}{v_{j,cat}}$ , where

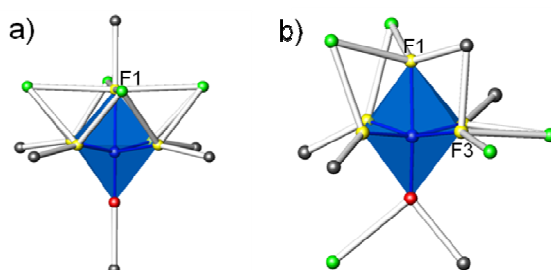
z<sub>j,cat</sub> is the electric charge of each A<sub>i</sub> alkali cation bonded to a given ligand and v<sub>j,cat</sub> is its coordination number; <sup>c</sup> Cationic BV sum = Σ<sub>i</sub> S<sub>i,cat</sub>, where S<sub>i,cat</sub> is taken from Table 2 for each A<sub>i</sub>–O/F bond.

The observation that the O1 site in  $\text{KNaNbOF}_5$  makes one cationic contact to  $\text{Na}^+$  in the extended bond network is understandable when other crystal chemistry factors are considered. The polarizability of the oxide ( $6.49 \text{ \AA}^3$ ) and fluoride ( $1.57 \text{ \AA}^3$ ) ions [29] also influences their interactions with the extended bond network. For instance, the “harder” (relative to oxide) F2 *trans* fluoride interacts with one  $\text{Na}^+$  ( $2.3501(14) \text{ \AA}$ ) and four  $\text{K}^+$  ( $2.9586(9) \text{ \AA}$ ) cations (Tables 2 and 3). Although there are fewer Na–F bonds compared to K–F, the Na–F interactions are much stronger, as seen by their shorter bond lengths and higher bond valences. Thus, the  $\text{Na}^+$  cation is significantly over bonded (1.22 vu) with respect to  $\text{K}^+$  (1.08 vu). The  $\text{K}^+$  cation is softer than  $\text{Na}^+$ , therefore it needs to make more contacts to the fluorides in order to satisfy PSCR. At the same time, the  $\text{Nb}^{5+}$  ion displaces away from the *trans* fluoride toward the “softer” oxide which has the lowest PSCR sum and bond valence sum of 0.17 and 0.26, respectively. As a result, the oxide attracts one  $\text{Na}^+$  in the extended bond network at  $2.2961(16) \text{ \AA}$  and is under bonded.

### 2.3. Centrosymmetry versus Noncentrosymmetry

$\text{KNaNbOF}_5$  has a noncentrosymmetric polymorph [20]. The results discussed here on the noncentrosymmetric polymorph can be found in [20]. The different local coordination environments around the centrosymmetric (CS) and noncentrosymmetric (NCS)  $[\text{NbOF}_5]^{2-}$  structures are illustrated in Figure 3. In the NCS polymorph the two fluorides F1 and F3 contain the largest residual negative charge (0.48 and 0.23 vu, respectively) and make three contacts with two eight-coordinate  $\text{K}^+$  and one six-coordinate  $\text{Na}^+$ . In the CS polymorph, one fluoride, F1, has the largest residual negative charge (0.58 vu) and makes four contacts with four twelve-coordinate  $\text{K}^+$  and one six-coordinate  $\text{Na}^+$ . Although there are fewer Na–F interactions than K–F in both the NCS and CS polymorphs, the Na–F interactions are stronger, as seen by their shorter bond lengths and higher bond valences. As a result, in the CS polymorph the  $\text{Na}^+$  cation is slightly more over bonded (1.22 vu) compared to  $\text{K}^+$  (1.08 vu).

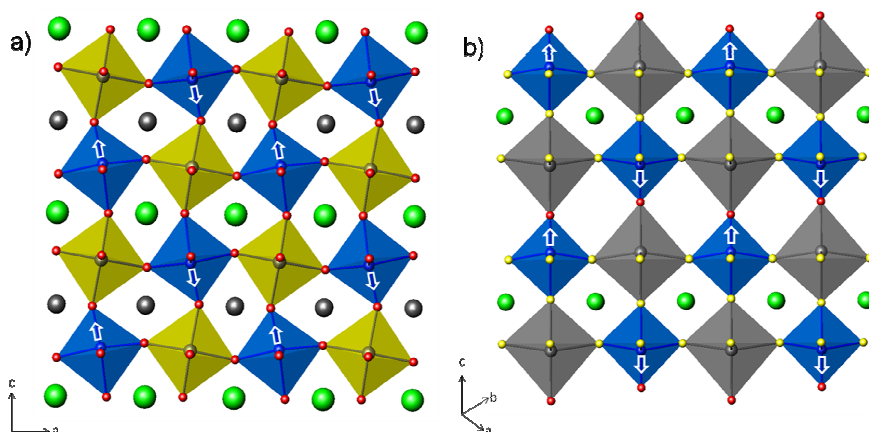
**Figure 3.** Cationic coordination environment around (a) the centrosymmetric (CS) polymorph and (b) the noncentrosymmetric (NCS) polymorph. Blue octahedra represents the  $[\text{NbOF}_5]^{2-}$  unit. The spheres represent  $\text{O}^{2-}$  (red),  $\text{F}^-$  (yellow),  $\text{Na}^+$  (black) and  $\text{K}^+$  (orange).



The oxides in both the NCS and CS polymorph are under bonded. In the NCS polymorph, the oxide is three-coordinate with one  $\text{K}^+$  and one  $\text{Na}^+$  contact and a Nb=O bond at  $1.745(5) \text{ \AA}$ . In the CS polymorph, the oxide is two-coordinate and makes one  $\text{Na}^+$  contact and as expected there is a shorter Nb=O bond distance of  $1.7179(14) \text{ \AA}$ . Conversely, the extra  $\text{K}^+$  contact in the NCS polymorph results in a longer Nb=O bond.

In a perovskite with B-site rock-salt ordering the A-site cations prefer to order in a layered arrangement which is stabilized by the presence of a second order Jahn Teller displacement of at least one  $d^0$  transition metal at the B-site [10,11]. In  $\text{NaLnMnWO}_6$  and  $\text{NaLnMgWO}_6$  with a trivalent and monovalent A-site cation, the oxides coordinated to the  $\text{Na}^+$  are under bonded while the oxides coordinated to the  $\text{Ln}^{3+}$  are over bonded. To compensate, the  $d^0$  transition metal,  $\text{W}^{6+}$ , at the B-site will shift towards the oxide coordinated to the smaller cation ( $\text{Na}^+$ ) and away from the larger cation ( $\text{Ln}^{3+}$ ) to alleviate the lattice strain arising from the size mismatch (Figure 4a). A similar comparison can be made to  $\text{KNaNbOF}_5$ . Instead of having two A-site cations, there is an occupied and unoccupied A-site. As a result, the oxide in the same layer as the unoccupied A-site is under bonded. To compensate, the  $\text{Nb}^{5+}$  at the B-site shifts toward the oxide and away from the *trans* fluoride (Figure 4b). Thus, the long range ordering of the  $\text{KNaNbOF}_5$  structure results in a centrosymmetric arrangement of the anionic units.

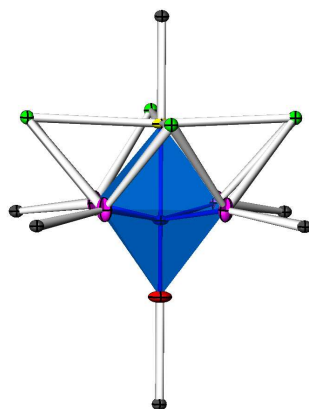
**Figure 4.** The  $d^0$  transition metal (blue) at the B-site shifts towards the oxide that contains the smallest A-site cation, Na (grey) for (a)  $\text{NaLaMnWO}_6$  [10,11] or the vacancy in (b)  $\text{KNaNbOF}_5$ .



#### 2.4. $\text{KNaMO}_2\text{F}_4$ and partial anionic ordering

In  $\text{KNaMO}_2\text{F}_4$  ( $M = \text{Mo}^{6+}, \text{W}^{6+}$ ), the oxide and its *trans* fluoride are ordered while the second oxide is disordered along with the other three fluorides at the equatorial positions. Despite the partial ordering of the oxide and fluoride, the A- and B-site cations are ordered. The partial ordering of the anionic unit has been reported previously, where Mo/W distorts towards the corner as opposed to the edge [22,23]. The partial ordering of the oxide and fluoride is due to the symmetric environment around the equatorial positions. In  $\text{KNaNbOF}_5$ , the bond network at the oxide differs from the *trans* fluoride; therefore, the oxide can be identified based on bond lengths. When two oxides are present as in  $\text{KNaMO}_2\text{F}_4$ , one oxide is ordered (Figure 5). The bond lengths of the oxide and the *trans* fluoride at the axial positions are different, which we use to identify the oxide and fluoride sites. However, at the equatorial positions, the bond length is the average of the four bonds from the second oxide and three fluorides, therefore the second oxide and three fluorides are not differentiated. In addition, bond valence sums cannot be accurately calculated because it is dependent on the observed bond lengths.

**Figure 5.** Cationic coordination environment around  $\text{KNaMoO}_2\text{F}_4$ . Blue octahedra represents the  $[\text{MOF}_5]^{2-}$  unit (no tilt,  $a^0a^0a^0$ ). The ellipsoids represent  $\text{O}^{2-}$  (red),  $\text{F}^-$  (yellow),  $\text{O}^{2-}/\text{F}^-$  (purple),  $\text{Na}^+$  (black) and  $\text{K}^+$  (orange).



### 3. Experimental Section

#### 3.1. Materials and synthesis

**Caution:** Hydrofluoric acid is toxic and corrosive, and must be handled with extreme caution and the appropriate protective gear! If contact with the liquid or vapor occurs, proper treatment procedures should immediately be followed [30-32].

**Materials:**  $\text{Nb}_2\text{O}_5$  (99.9%, Aldrich),  $\text{Na}_2\text{MoO}_4 \cdot 2\text{H}_2\text{O}$  (99.9%, Aldrich),  $\text{Na}_2\text{WO}_4 \cdot 2\text{H}_2\text{O}$  (99.9%, Aldrich),  $\text{NaF}$  (99.9%, Aldrich),  $\text{KF}$  (99.9%, Aldrich), and aqueous hydrofluoric acid (HF) (48% HF by weight, Aldrich) were used as received. Owing to their hygroscopic nature, the alkali fluorides were weighed under nitrogen in a dry box.

All reactants were sealed in Teflon [fluoro(ethylenepropylene), FEP] “pouches” [33]. Single or multiple pouches were placed in a 125 mL Teflon-lined Parr pressure vessel filled 33% with deionized  $\text{H}_2\text{O}$  as backfill [34]. The pressure vessel was heated for 24 h at 150 °C and cooled to room temperature over an additional 24 h. The pouches were opened in air, and the products were recovered by vacuum filtration.

**$\text{KNaNbOF}_5$ .**  $\text{KNaNbOF}_5$  was synthesized by reacting  $\text{NaF}$  (0.0790g, 0.0019 mol),  $\text{KF}$  (0.1639g, 0.0028 mol),  $\text{Nb}_2\text{O}_5$  (0.25g, 0.0009 mol) and 48% aqueous HF (0.5000 g, 0.0250 mol). Colorless plates were recovered in 68% yield based on Nb.

**$\text{KNaMoO}_2\text{F}_4$ .**  $\text{KNaMoO}_2\text{F}_4$  was synthesized by reacting  $\text{KF}$  (0.0600g, 0.0010 mol),  $\text{Na}_2\text{MoO}_4 \cdot 2\text{H}_2\text{O}$  (0.25g, 0.0010 mol) and 48% aqueous HF (0.2500 g, 0.0125 mol). Colorless plates were recovered in 66% yield based on Mo.

**$\text{KNaWO}_2\text{F}_4$ .**  $\text{KNaWO}_2\text{F}_4$  was synthesized by reacting  $\text{KF}$  (0.0440g, 0.0008 mol),  $\text{Na}_2\text{WO}_4 \cdot 2\text{H}_2\text{O}$  (0.25g, 0.0008 mol) and 48% aqueous HF (0.2500 g, 0.0125 mol). Colorless plates were recovered in 72% yield based on W.

### 3.2. Crystallographic determination

Single crystal X-ray diffraction data of  $\text{KNaNbOF}_5$ ,  $\text{KNaMoO}_2\text{F}_4$  and  $\text{KNaWO}_2\text{F}_4$  were collected with Mo-K $\alpha$  radiation (0.71073 Å) on a Bruker APEX2 CCD diffractometer and integrated with the SAINT-Plus program [35]. The structures were solved by direct methods and refined against  $F^2$  by full-matrix least-squares techniques with SHELX. A face-indexed absorption correction was performed numerically using the program XPREP. All structures were checked for missing symmetry elements with PLATON [36]. The final refinement includes anisotropic displacement parameters. Further details of the crystal structure investigations may be obtained from Fachinformationszentrum Karlsruhe, 76344 Eggenstein-Leopoldshafen, Germany (fax: (+49)7247-808-666; e-mail: crysdata@fiz-karlsruhe.de, [http://www.fiz-karlsruhe.de/request\\_for\\_deposited\\_data.html](http://www.fiz-karlsruhe.de/request_for_deposited_data.html)) on quoting the 422708 ( $\text{KNaNbOF}_5$ ), 422707 ( $\text{KNaMoO}_2\text{F}_4$ ) and 422709 ( $\text{KNaWO}_2\text{F}_4$ ) CSD numbers. Crystallographic data for  $\text{KNaNbOF}_5$  and  $\text{KNaMO}_2\text{F}_4$ , ( $M = \text{Mo}^{6+}$ ,  $\text{W}^{6+}$ ) are given in Table 4.

**Table 4.** Crystallographic Data for  $\text{KNaNbOF}_5$ ,  $\text{KNaMoO}_2\text{F}_4$  and  $\text{KNaWO}_2\text{F}_4$ .

Formula	$\text{KNaNbOF}_5$	$\text{KNaMoO}_2\text{F}_4$	$\text{KNaWO}_2\text{F}_4$
fw	266.00	266.03	353.94
Space group	P4/nmm (No. 129)	P4/nmm (No. 129)	P4/nmm (No. 129)
a (Å)	5.91390(10)	5.8600(2)	5.86350(10)
c (Å)	8.5114(2)	8.45960(10)	8.49070(10)
V(Å <sup>3</sup> )	297.680(10)	290.499(3)	219.916(8)
Z	2	2	2
T(K)	100(2)	100(2)	100(2)
$\lambda$ (Å)	0.71073	0.71073	0.71073
$\rho_{\text{calc}}$ (g/cm <sup>3</sup> )	2.968	3.041	4.027
$\mu$ (mm <sup>-1</sup> )	2.812	3.055	20.579
R(F) <sup>a</sup>	0.0102	0.0163	0.0111
wR <sub>2</sub> (F <sub>2</sub> ) <sup>b</sup>	0.0274	0.0342	0.0248

<sup>a</sup>  $R = \sum ||F_o| - |F_c|| / \sum |F_o|$ ; <sup>b</sup>  $wR_2 = [\sum w(F_o^2 - F_c^2)^2 / \sum w(F_o^2)^2]^{1/2}$

### 3.3. Spectroscopic measurements

Mid-infrared (600–4000 cm<sup>-1</sup>) spectra of  $\text{KNaNbOF}_5$ ,  $\text{KNaMoO}_2\text{F}_4$  and  $\text{KNaWO}_2\text{F}_4$  were collected using a Bruker 37 Tensor FTIR spectrometer equipped with an ATR germanium cell attachment operating at a resolution of 2 cm<sup>-1</sup>.

## 4. Conclusions

The interactions of the  $[\text{NbOF}_5]^{2-}$  and  $[\text{MO}_2\text{F}_4]^{2-}$  anionic units with the cationic bond network ( $\text{Na}^+$  and  $\text{K}^+$ ) influences the long range ordering of the anionic units. The oxide coordinated to the unoccupied A-sites is under bonded. To compensate, the d<sup>0</sup> transition metal (Nb/M) shifts towards the oxide coordinated to the unoccupied A-site and away from the fluoride coordinated to the  $\text{K}^+$  to satisfy PSCR. These interactions in  $\text{KNaNbOF}_5$  and  $\text{KNaMO}_2\text{F}_4$  lead to a rock salt ordering of the B-site cations and an ordered layering of the occupied and unoccupied A-sites resulting in a centrosymmetric arrangement.

## Acknowledgements

The authors thank Michael R. Marvel for valuable insights and discussions and Martin Donakowski for the IR measurements of  $\text{KNaNbOF}_5$ ,  $\text{KNaMoO}_2\text{F}_4$  and  $\text{KNaWO}_2\text{F}_4$ . The authors gratefully acknowledge the support from the National Science Foundation (Solid State Chemistry Award Nos. DMR-0604454 and DMR-1005827) and the use of the Central Facilities supported by the MRSEC program of the National Science Foundation (DMR-0076097 and DMR-0520513) at the Materials Research Center of Northwestern University.

## References and Notes

1. Shimakawa, Y. A-Site Ordered Perovskites with Intriguing Physical Properties. *Inorg. Chem.* **2008**, *47*, 8562-8570.
2. Stramare, S.; Thangadurai, V.; Weppner, W. Lithium Lanthanum Titanates: A Review. *Chem. Mater.* **2003**, *15*, 3974-3990.
3. Brink, F.J.; Norén, L.; Goossens, D.J.; Withers, R.L.; Liu, Y.; Xu, C.-N. A combined diffraction (XRD, electron and neutron) and electrical study of  $\text{Na}_3\text{MoO}_3\text{F}_3$ . *J. Solid State Chem.* **2003**, *174*, 450-458.
4. Woodward, P.M.; Karen, P. Mixed Valence in  $\text{YBaFe}_2\text{O}_5$ . *Inorg. Chem.* **2003**, *42*, 1121-1129.
5. Chakhmouradian, A.R.; Mitchell, R.H.; Burns, P.C. The A-site deficient ordered perovskite  $\text{Th}_{0.25}\square_{0.75}\text{NbO}_3$ : a re-investigation. *J. Alloys Compounds* **2000**, *307*, 149-156.
6. Iyer, P.N.; Smith, A.J. Double Oxides Containing Niobium, Tantalum, or Protactinium. III. Systems Involving the Rare Earths. *Acta Crystallogr.* **1967**, *23*, 740.
7. Kennedy, B.J.; Howard, C.J.; Kubota, Y.; Kenichi, K. Phase transition behavior in the A-site deficient perovskite oxide  $\text{La}_{1/3}\text{NbO}_3$ . *J. Solid State Chem.* **2004**, *177*, 4552-4556.
8. Sefat, A.S.; Amow, G.; Wu, M.-Y.; Botton, G.A.; Greedan, J.E. High-resolution EELS study of the vacancy-doped metal/insulator system,  $\text{Nd}_{1-x}\text{TiO}_3$ ,  $x = 0$  to 0.33. *J. Solid State Chem.* **2005**, *178*, 1008-1016.
9. Dupont, L.; Chai, L.; Davies, P.K. A- and B-site ordered in  $(\text{Na}_{1/2}\text{La}_{1/2})(\text{Mg}_{1/3}\text{Ta}_{2/3})\text{O}_3$  Perovskites. *Mater. Res. Soc. Symp. P.* **1998**, *547*, 93-98.
10. King, G.; Wayman, L.M.; Woodward, P.M. Magnetic and structural properties of  $\text{NaLnMnWO}_6$  and  $\text{NaLnMgWO}_6$ . *J. Solid State Chem.* **2009**, *182*, 1319-1325.
11. Knapp, M.C.; Woodward, P.M. A-site cation ordering in  $\text{AA}'\text{BB}'\text{O}_6$  perovskites. *J. Solid State Chem.* **2006**, *179*, 1076-1085.
12. Anderson, M.T.; Greenwood, K.B.; Taylor, G.A.; Poeppelmeier, K.R. B-Cation Arrangements in Double Perovskites. *Prog. Solid State Chem.* **1993**, *22*, 197-233.
13. Howard, C.J.; Kennedy, B.J.; Woodward, P.M. Ordered double perovskites - a group-theoretical analysis. *Acta Crystallogr. B* **2003**, *59*, 463-471.
14. Lufaso, M.W.; Barnes, P.W.; Woodward, P.M. Structure prediction of ordered and disordered multiple octahedral cation perovskites using SPuDS. *Acta Crystallogr. B* **2006**, *62*, 397-410.

15. Barnes, P.W.; Lufaso, M.W.; Woodward, P.M. Structure determination of  $A_2M^{3+}TaO_6$  and  $A_2M^{3+}NbO_6$  ordered perovskites: octahedral tilting and pseudosymmetry. *Acta Crystallogr. B* **2006**, *62*, 384-396.
16. Woodward, P.; Hoffmann, R.D.; Sleight, A.W. Order-disorder in  $A_2M^{3+}M^{5+}O_6$  perovskites. *J. Mater. Res.* **1994**, *9*, 2118-2127.
17. Flerov, I.N.; Gorev, M.V.; Tressaud, A.; Laptash, N.M. Perovskite-Like Fluorides and Oxyfluorides: Phase Transitions and Caloric Effects. *Crystallogr. Rep.* **2011**, *56*, 9-17.
18. Vasiliev, A.D.; Zaitsev, A.; Cherepakhin, A.V.; Laptash, N.M. Polymorphic Modification of Crystal  $SrB_4O_7$  and  $KNaNbOF_5$ . *Phase Transit., Ordered State., New Mater.* **2010**, *11*, 2.
19. Izumi, H.K.; Kirsch, J.E.; Stern, C.L.; Poeppelmeier, K.R. Examining the Out-of-Center Distortion in the  $[NbOF_5]^{2-}$  Anion. *Inorg. Chem.* **2005**, *44*, 884-895.
20. Marvel, M.R.; Lesage, J.; Baek, J.; Halasyamani, P.S.; Stern, C.L.; Poeppelmeier, K.R. Cation-Anion Interactions and Polar Structures in the Solid State. *J. Am. Chem. Soc.* **2007**, *129*, 13963-13969.
21. Pausewang, G.; Schmitt, R.; Dehnicke, K. Vibrational-Spectra of Oxofluoro Complexes of Species  $NbOF_5^{2-}$ ,  $TaOF_5^{2-}$ ,  $MoO_2F_4^{2-}$ ,  $WO_2F_4^{2-}$ ,  $NbOF_6^{3-}$ , and  $MoO_2F_5^{3-}$ . *Z. Anorg. Allg. Chem.* **1974**, *408*, 1-8.
22. Heier, K.R.; Norquist, A.J.; Halasyamani, P.S.; Duarte, A.; Stern, C.L.; Poeppelmeier, K.R. The polar  $[WO_2F_4]^{2-}$  anion in the solid state. *Inorg. Chem.* **1999**, *38*, 762-767.
23. Marvel, M.R.; Pinlac, R.A.F.; Lesage, J.; Stern, C.L.; Poeppelmeier, K.R. Chemical Hardness and the Adaptive Coordination Behavior of the  $d^0$  Transition Metal Oxide Fluoride Anions. *Z. Anorg. Allg. Chem.* **2009**, *635*, 869-877.
24. Pauling, L. The principles determining the structure of complex ionic crystals. *J. Am. Chem. Soc.* **1929**, *51*, 1010-26.
25. Tobias, G.; Beltran-Porter, D.; Lebedev, O.I.; Van Tendeloo, G.; Rodriguez-Carvajal, J.; Fuertes, A. Anion Ordering and Defect Structure in Ruddlesden-Popper Strontium Niobium Oxynitrides. *Inorg. Chem.* **2004**, *43*, 8010-8017.
26. Brown, I.D.; Altermatt, D. Bond-valence parameters obtained from a systematic analysis of the inorganic crystal structure database. *Acta Crystallogr. B Struct. Sci.* **1985**, *B41*, 244-247.
27. Brown, I.D. *The Chemical Bond in Inorganic Chemistry: The Bond Valence Model*, 1st ed.; Oxford University Press: Oxford, UK, 2002; Volume 1, p. 278.
28. Brown, I.D. Recent developments in the bond valence model of inorganic bonding. *Phys. Chem. Miner.* **1987**, *15*, 30-34.
29. Shannon, R.D.; Fischer, R.X. Empirical electronic polarizabilities in oxides, hydroxides, oxyfluorides, and oxychlorides. *Phys. Rev. B* **2006**, *73*, 235111.
30. Bertolini, J.C. Hydrofluoric acid: a review of toxicity. *J. Emerg. Med.* **1992**, *10*, 163-168.
31. Peters, D.; Miethchen, R. Symptoms and treatment of hydrogen fluoride injuries. *J. Fluorine Chem.* **1996**, *79*, 161-165.
32. Segal, E.B. First aid for a unique acid, HF: A sequel. *Chem. Health Safety* **2000**, *7*, 18-23.
33. Harrison, W.T.A.; Nenoff, T.M.; Gier, T.E.; Stucky, G.D. Tetrahedral-atom 3-ring groupings in 1-dimensional inorganic chains: beryllium arsenate hydroxide hydrate ( $Be_2AsO_4OH \cdot 4H_2O$ ) and

sodium zinc hydroxide phosphate hydrate ( $\text{Na}_2\text{ZnPO}_4\text{OH}\cdot 7\text{H}_2\text{O}$ ). *Inorg. Chem.* **1993**, *32*, 2437-2441.

34. Norquist, A.J.; Heier, K.R.; Stern, C.L.; Poeppelmeier, K.R. Composition space diagrams for mixed transition metal oxide fluorides. *Inorg. Chem.* **1998**, *37*, 6495-6501.
35. Bruker Analytical X-ray Instruments, Inc. *SAINTE-Plus*, version 6.02A; Bruker Analytical X-ray Instruments, Inc.: Madison, WI, USA, 2000.
36. Spek, A.L. *PLATON*; Utrecht University: Utrecht, The Netherlands, 2001.

© 2011 by the authors; licensee MDPI, Basel, Switzerland. This article is an open access article distributed under the terms and conditions of the Creative Commons Attribution license (<http://creativecommons.org/licenses/by/3.0/>).